Letters

A Single Sampling Double Update Modulation Method to Enhance Low-Carrier Ratio Operation

Chun Wu, Chunqiao Zhu, and Luhua Zheng

***Abstract*—To solve problems of low-accuracy synthetic voltage vector, large current ripple, and poor stability in sensor/sensorless control of permanent-magnet synchronous motors (PMSMs) under low-carrier ratio operations, a single sampling double update space vector pulsewidth modulation (SSDU-SVPWM) is proposed. In this method, the phase current is sampled only once, however the target voltage vector is calculated once but update twice in one PWM period. Each PWM period is divided into the first half and the second half. Two voltage vectors with the same amplitude and different delay angles are executed in the first and the second half, respectively. In comparison with the traditional method of compensating an average delay angle of $1.5T_s$, the proposed SSDU-SVPWM compensates $1.25T_s$ and $1.75T_s$ for the first half and the second half sequentially. It reduces the synthetic error of the target voltage vector, lowers the phase-current ripple, and improves the efficiency and stability of the system. Finally, the effectiveness of the proposed scheme was verified both on sensor and sensorless control of PMSMs.**

***Index Terms*—Low-carrier ratio, permanent-magnet synchronous motor, single sampling double update, space vector pulsewidth modulation (SVPWM).**

I. Introduction

PERMANENT-MAGNET synchronous motors (PMSMs) have been widely used in high-speed and high-power applications, such as vacuum cleaners, electric vehicle motors, and so on because of their high efficiency and high reliability. The carrier ratio is defined as a ratio of pulsewidth modulation (PWM) frequency (f_{pwm}) to motor fundamental frequency (f_{e}), i.e., $N_{\mathrm{ratio}} = f_{\mathrm{pwm}} / f_{\mathrm{e}}$. Implementing stable and efficient operations of PMSM under low-carrier ratio has important research and application value. In practical applications, the switching frequency of the power semiconductor is usually limited (below 30 kHz) due to the constraint of power switches [1], [2]. When the carrier ratio decreases with the increase of motor speed, both the phase delay and the output voltage amplitude attenuation caused by the digital delay of the processor and the update delay of the inverter will be magnified, resulting in increases of the current/torque ripple, the *dq*-axes current coupling, and the instability of the system.

To improve the stability of the system under low-carrier ratio, many literatures have presented fruitful achievements in designing current-loop controller, shortening sampling time, reducing the harmonic effect, optimizing space vector pulsewidth modulation (SVPWM) and so on. To reduce current coupling, an improved method for complex vector decoupling is proposed in [3] and [4], which improves the dynamic characteristics of the current loop. The influence of the current single sampling PWM single update (SSSU) is analyzed and a compensation with a $1.5T_s$ average time delay is proposed in [5], which is verified extensively and widely adopted in nowadays motor drives. In comparison, the double current sampling and double PWM update (DSDU) can reduce the delay time by half, i.e., $0.75T_s$, and can reach a lower carrier ratio operation [6]. Recently, a multisampling and PWM multiupdating (MSMU) method is proposed, which samples *N* times current and compares the new update target voltage with the carrier wave in one switching cycle to reduce digital delay [7], [8]. Later, adopting the principle of the MSMU, an improved deadbeat control of PMSMs samples the phase current at a very high frequency, 1 MHz, and calculates the desired output voltage at every sampling instant, which can reduce the digital delay into $0.25T_s$ to $0.75T_s$. Hence, it achieves smaller current ripple and lowers total harmonic distortion (THD) [9]. Furthermore, a simplified attempt is to sample phase current four times and update PWM twice in one switching cycle to enhance the high-speed operation of PMSM drives, in which the digital delay is reduced to $0.5T_s$ [10]. Nevertheless, the aforementioned methods almost require isolated current sensors, fast analog-to-digital converters (ADC) and advanced control chips, such as field-programmable gate arrays (FPGAs), which needs higher cost, larger printed circuit board, heavier calculations, and will not be adopted in low-cost drives.

Plenty of literatures improve the PMSM control performance under low-carrier ratio by optimizing the current controller or reducing the sampling and control delay. However, most of them require expensive hardware. From another aspect, the SVPWM strategy maybe be modified, and then, a precise voltage can be generated to reduce the synthetic error. One solution is to design

Manuscript received 1 September 2023; revised 12 October 2023; accepted 31 October 2023. Date of publication 3 November 2023; date of current version 22 December 2023. This work was supported in part by the National Natural Science Foundation of China under Grant 52007169 and in part by the Natural Science Foundation of Zhejiang Province under Grant LY23E070004. *(Corresponding author: Chun Wu.)*

The authors are with the College of Information Engineering, Zhejiang University of Technology, Hangzhou 310000, China (e-mail: wuchun@zjut.edu.cn; 2112103068@zjut.edu.cn; 2112003028@zjut.edu.cn).

Color versions of one or more figures in this article are available at https://doi.org/10.1109/TPEL.2023.3329953.

Digital Object Identifier 10.1109/TPEL.2023.3329953

optimized modulation methods to reduce current harmonics under low-carrier ratio, include an online calculation SVPWM [11], a current harmonic minimization SVPWM [12], and a multimode SVPWM [13], etc. Nevertheless, these methods only operate switching angles, cannot reduce the voltage synthetic error. Another attempt is to divide a PWM period into three equal parts, and every part has its own voltage vector to reduce the voltage synthetic error. This method can reduce the current THD and torque ripple in the deadbeat predictive torque control for PMSM drives [14]. However, it will cause more switching times and increase switching loss. Furthermore, a novel SVPWM strategy is proposed in [15], which can reduce the error of synthetic voltage vector under low-carrier ratio. This method at most requires three synthetic voltage vectors in one PWM period. Nevertheless, this method has a big disadvantage of complex calculation, and does not consider a smooth transition between different vector switching in one PWM period, resulting in a fluctuation of phase current during the vector switching.

Aiming at these problems of weak stability, complex implementation, and poor robustness to motor parameters under low-carrier ratio, this letter proposes a single sampling double update SVPWM (SSDU-SVPWM) to enhance the low-carrier ratio operation. The key idea of this method is to consider the motor rotation speed in the first and the second half of a PWM period. Then, different delay angles are compensated with respect to each half, which means that two voltage vectors with the same magnitude, but different phases are executed in the first and the second half. It can reduce the voltage error caused by motor rotation and improve the stability of the system under low-carrier ratio. Finally, the effectiveness of the proposed method is verified in both sensor and sensorless control drives.

II. Proposed SSDU-SVPWM

In this section, we will analyze the difference between the traditional SVPWM and the proposed SSDU-SVPWM from two aspects of phase delay compensation and voltage amplitude attenuation and give the implementation of the SSDU-SVPWM.

A. Conventional Single Sampling Single Update Modulation

Due to PWM execution delay from the PWM calculation to the voltage really acts on the motor is from T_s to $2T_\mathrm{s}$. According to the conventional average angle compensation in [5], an average compensation angle $1.5T_\mathrm{s}$ consisting of one T_s digital control delay and a half T_s inverter delay, where T_s is the PWM cycle.

As shown in Fig. 1, rotating synchronous coordinate frames of sampling time kT_s and delay $kT_\mathrm{s}+1.25T_\mathrm{s}$, $kT_\mathrm{s}+1.5T_\mathrm{s}$, and $kT_\mathrm{s}+1.75T_\mathrm{s}$ are represented by $d_s\ q_s$, $d_i\ q_i$, $d_a\ q_a$, and $d_f\ q_f$, respectively. The output voltage vectors corresponding to $d_s\ q_s$, $d_i\ q_i$, $d_a\ q_a$, and $d_f\ q_f$ coordinate systems are $\boldsymbol{v}_\mathrm{s}, \boldsymbol{v}_\mathrm{s}^i, \boldsymbol{v}_\mathrm{s}^a$, and $\boldsymbol{v}_\mathrm{s}^f$, respectively. The voltage transformation from dq-axes to $\alpha\beta$-axes is given by

$$\boldsymbol{u}_{\alpha\beta}^* = \boldsymbol{u}_{dq}^* e^{j\theta_\mathrm{e}} \tag{1}$$

where $\boldsymbol{u}_{dq}^*$ represents the given voltage, $\boldsymbol{u}_{\alpha\beta}^*$ represents the expected voltage applied to the motor, and θ_e represents angle between the dq-axes and the $\alpha\beta$-axes.

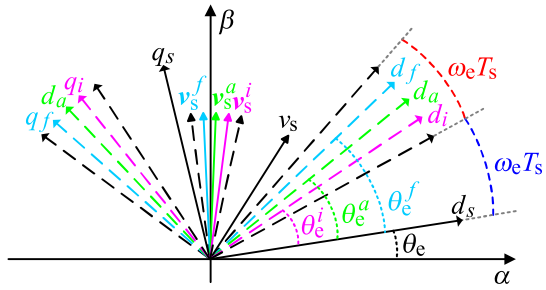

Fig. 1. Rotating synchronous reference frames corresponding to each time sequence.

As shown in [5], for the SSSU modulation, the voltage amplitude attenuation, and the average delay angle in the inverter delay interval $[T_\mathrm{s},\ 2T_\mathrm{s}]$ can be derived as

$$\begin{aligned}\bar{\boldsymbol{u}}_{\alpha\beta}^* &= \frac{1}{T_s}\int_{T_\mathrm{s}}^{2T_\mathrm{s}} \boldsymbol{u}_{dq}^* e^{j(\omega_\mathrm{e}\tau+\theta_\mathrm{e})} d\tau \\ &= K_u^a \cdot e^{j(\theta_\mathrm{e}^a+\theta_\mathrm{e})} \boldsymbol{u}_{dq}^*\end{aligned} \tag{2}$$

where K_u^a and θ_e^a are the voltage amplitude attenuation factor and average delay angle of interval $[T_\mathrm{s},\ 2T_\mathrm{s}]$, respectively. The voltage amplitude attenuation factor K_u^a is defined as a ratio of the achieved voltage to the expected voltage.

$$\begin{cases} K_u^a = \frac{2}{T_\mathrm{s}\omega_\mathrm{e}} \sin\left(\frac{\omega_\mathrm{e}T_\mathrm{s}}{2}\right) \\ \theta_\mathrm{e}^a = 1.5T_\mathrm{s}\omega_\mathrm{e} \end{cases} \tag{3}$$

where ω_e and θ_e represents the speed and angle used by the controller, respectively. $\boldsymbol{u}_{dq}^*$ represents the given voltage, and $\bar{\boldsymbol{u}}_{\alpha\beta}^*$ represents the average voltage applied to the motor. The superscript a is the average of interval $[T_\mathrm{s},\ 2T_\mathrm{s}]$.

B. Proposed Single Sampling Double Update SVPWM

As shown in Fig. 1, the inverter delay interval $[T_\mathrm{s},\ 2T_\mathrm{s}]$ is divided into two parts: $[T_\mathrm{s},\ 1.5T_\mathrm{s}]$ and $[1.5T_\mathrm{s},\ 2T_\mathrm{s}]$. The voltage amplitude attenuation and delay angle of these two half delay intervals can be calculated as

$$\begin{aligned}\bar{\boldsymbol{u}}_{\alpha\beta}^* &= \frac{1}{T_s}\left(\int_{T_\mathrm{s}}^{1.5T_\mathrm{s}} \boldsymbol{u}_{dq}^* e^{j(\omega_\mathrm{e}\tau+\theta_\mathrm{e})} d\tau \right. \\ &\quad \left. + \int_{1.5T_\mathrm{s}}^{2T_\mathrm{s}} \boldsymbol{u}_{dq}^* e^{j(\omega_\mathrm{e}\tau+\theta_\mathrm{e})} d\tau\right) \\ &= K_u^i \cdot e^{j\left(\theta_\mathrm{e}^i+\theta_\mathrm{e}\right)} \boldsymbol{u}_{dq}^* + K_u^i \cdot e^{j\left(\theta_\mathrm{e}^f+\theta_\mathrm{e}\right)} \boldsymbol{u}_{dq}^*\end{aligned} \tag{4}$$

$$\begin{cases} K_u^i = \frac{4}{T_\mathrm{s}\omega_\mathrm{e}} \sin\left(\frac{\omega_\mathrm{e}T_\mathrm{s}}{4}\right) \\ \theta_\mathrm{e}^i = 1.25T_\mathrm{s}\omega_\mathrm{e} \\ \theta_\mathrm{e}^f = 1.75T_\mathrm{s}\omega_\mathrm{e} \end{cases} \tag{5}$$

where K_u^i is the voltage amplitude attenuation factor of interval $[T_\mathrm{s},\ 1.5T_\mathrm{s}]$ and $[1.5T_\mathrm{s},\ 2T_\mathrm{s}]$, and θ_e^i and θ_e^f are the average delay angles of intervals $[T_\mathrm{s},\ 1.5T_\mathrm{s}]$ and $[1.5T_\mathrm{s},\ 2T_\mathrm{s}]$, respectively.

To implement the compensation algorithm of the SSDU-SVPWM, only the voltage amplitude attenuation and delay angles need to be compensated with respect to each half interval,

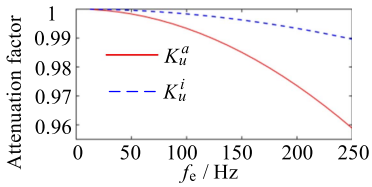

Fig. 2. Curves of voltage amplitude attenuation factor.

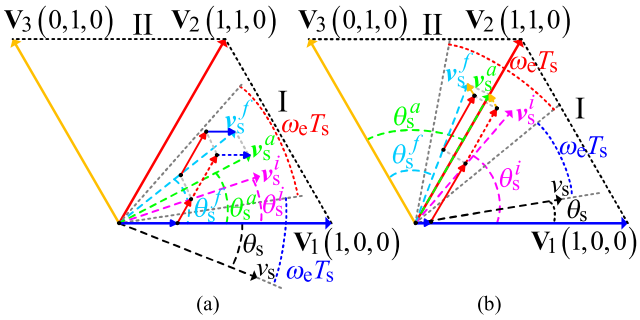

Fig. 3. Vector synthesis of the SSDU-SVPWM. (a) Same sector. (b) Different sectors.

expressed as

$$\boldsymbol{u}_{dq}^{**} = \frac{\boldsymbol{u}_{dq}^{*}}{K_u^i}, [T_s, 2T_s] \tag{6}$$

$$\theta_e^{**} = \begin{cases} \theta_e + \theta_e^i, & [T_s, 1.5T_s] \\ \theta_e + \theta_e^f, & [1.5T_s, 2T_s] \end{cases} \tag{7}$$

where $\boldsymbol{u}_{dq}^{**}$ is the given voltage after the compensation, and θ_e^{**} is the angle used for inverse Park transformation after compensation.

C. Voltage Amplitude Attenuation Analysis

The relationship of the voltage amplitude attenuation factor between the traditional method and the proposed method can be derived as

$$\mu = \frac{K_u^a}{K_u^i} = \cos\left(\frac{\omega_e T_s}{4}\right) \tag{8}$$

where μ is the amplitude attenuation ratio of the aforementioned two methods. When $0 \le \omega_e T_s \le 2\pi, 0 \le m \le 1$, the K_u^a is always smaller than the K_u^i. The SSDU-SVPWM can improve the voltage amplitude attenuation problem caused by low-carrier ratio and reduce the phase current ripple and torque ripple. The curves of the attenuation factor with respect to the change of velocity at $f_{\text{pwm}} = 1$ kHz are shown in Fig. 2.

D. Switching Sequence of SSDU-SVPWM

Fig. 3 shows the steps of voltage synthesis, the $\boldsymbol{v}_s^i$ and $\boldsymbol{v}_s^f$ vectors are synthesized by the first and second half PWM cycle, respectively. Then, these two vectors can be combined into the average vector $\boldsymbol{v}_s^a$ in the traditional method. Fig. 3(a) and (b) corresponds to the switch sequences of Fig. 4(a) and (b), respectively. Fig. 4 shows the asymmetric PWM waveforms in the same sector (the $\boldsymbol{v}_s^i$ and $\boldsymbol{v}_s^f$ are in the same sector)

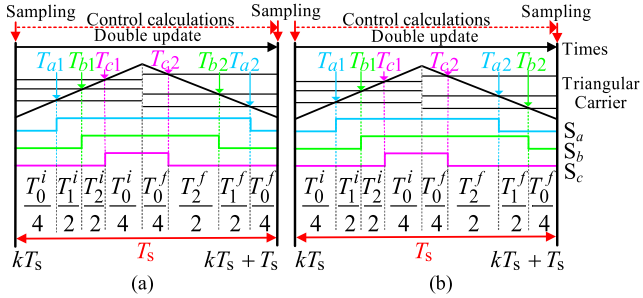

Fig. 4. Switch sequences of the SSDU-SVPWM. (a) Same sector. (b) Different sectors.

and different sectors (the $\boldsymbol{v}_s^i$ and $\boldsymbol{v}_s^f$ are in different sectors). According to the average value equivalent principle, the output voltage vector within a switching period T_s can be synthesized from some zero vectors and nonzero vectors [16]. The vector action time of the SSDU-SVPWM are calculated by (9)–(11).

1) Calculate vector angles for the first and second half PWM cycle as follows:

$$\begin{cases} \theta_s^i = \theta_s + 1.25 T_s \omega_e \\ \theta_s^f = \theta_s + 1.75 T_s \omega_e \end{cases}. \tag{9}$$

2) Calculate the action time for active vectors and zero vectors as follows:

$$\begin{cases} T_1^i = m T_s \sin\left(\frac{\pi}{3} - \theta_s^i\right) \\ T_2^i = m T_s \sin\theta_s^i \\ T_0^i = T_s - T_1^i - T_2^i \end{cases} \tag{10}$$

$$\begin{cases} T_1^f = m T_s \sin\left(\frac{\pi}{3} - \theta_s^f\right) \\ T_2^f = m T_s \sin\theta_s^f \\ T_0^f = T_s - T_1^f - T_2^f \end{cases} \tag{11}$$

where the superscript i and f represent the first and the second half in one PWM cycle, respectively. Angles θ_s, θ_s^i, and θ_s^f represent angles between the voltage vector and the adjacent nonzero odd vector ($0 \le \theta_s < \pi/3$), where the nonzero odd vector are $\mathbf{V}_1$(1,0,0), $\mathbf{V}_3$(0,1,0), and $\mathbf{V}_5$(0,0,1). m is the modulation index defined by

$$m = \frac{\sqrt{3}\,|\boldsymbol{v}_{\text{out}}|}{U_{\text{dc}}} \tag{12}$$

where $\boldsymbol{v}_{\text{out}}$ is the output voltage vector and U_{dc} is the bus voltage.

III. Experimental Results

The block diagram of the whole control system is depicted in Fig. 5. To validate the effectiveness of the proposed method, an experimental platform is set up, shown in Fig. 6. The parameters of the test PMSM drive are listed in Table I. A comparative experiment is carried out in a digital signal processor (DSP) TMS320F28335 to compare the control performance of the proposed method with position sensor and sensorless control. The PWM frequency and the sample frequency are both 1 kHz, and the current is sampled by two shunt-resistors on low-side bridges. The model reference adaptive system (MRAS) speed

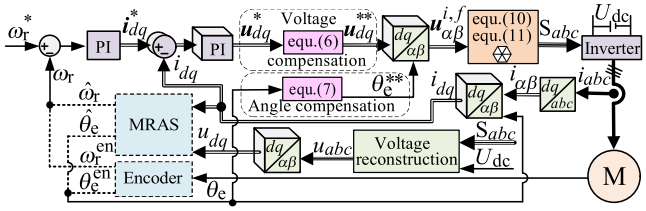

Fig. 5. SSDU-SVPWM control block diagram of the PMSM.

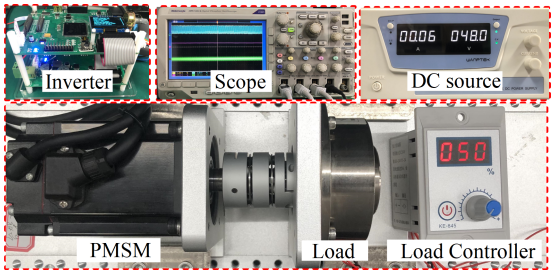

Fig. 6. Experimental platform.

TABLE I
PARAMETERS OF THE TEST PMSM

Parameters	Values	Parameters	Values
Rated voltage	48 V	Pole pairs	5
Rated current	10 A	Stator resistance	0.165 Ω
Rated speed	3000 r/min	*d*-axis inductance	0.181 mH
Rated torque	1.27 N·m	*q*-axis inductance	0.185 mH

observer is designed with a trapezoid Euler discretization [17]. The real position and speed obtained by 2500-line encoder are used for sensor control and comparison. The estimated position and speed of MRAS are used for sensorless control. ω_r^* is the given speed. θ_e^{en} and ω_r^{en} are the position and speed of the encoder, respectively. $\hat{\theta}_e$ and $\hat{\omega}_r$ are the estimated position and speed of MRAS, respectively. $\Delta\omega_r^{en}$ is the speed error within the sensor control and is denoted as $(\omega_r^{en} - \omega_r^*)$. $\Delta\hat{\theta}_e$ and $\Delta\omega_r^{en}$ are the position error and speed error in the sensorless control, respectively. $\Delta\hat{\theta}_e$ is denoted as $(\hat{\theta}_e - \theta_e^{en})$, and $\Delta\omega_r^{en}$ is denoted as $(\hat{\omega}_r - \omega_r^{en})$.

A. Steady-State Control Performance Test Experiment

To verify the steady-state control performance of the proposed SSDU-SVPWM, the following experiments at 2000 r/min ($N_{ratio} = 6$) under 50% rated load are implemented. The experimental results of the conventional method and the proposed SSDU-SVPWM based on sensor control are shown in Fig. 7(a) and (b), respectively. The speed error of the conventional method is 36.4 r/min, and the phase current is 16 A. Meanwhile, the speed error of the proposed method is 21.8 r/min, and the phase current is 14 A.

The experimental results of the conventional method and the proposed SSDU-SVPWM in sensorless control are shown in Fig. 8(a) and (b). The position estimation error of the conventional method is 8.8°, the speed estimation error is 27 r/min, and

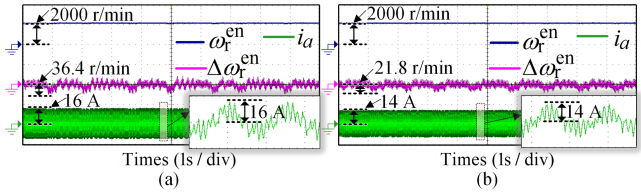

Fig. 7. Steady-state control performance of the sensor control at 2000 r/min ($N_{ratio} = 6$) under 50% rated load. (a) Conventional SVPWM. (b) Proposed SSDU-SVPWM.

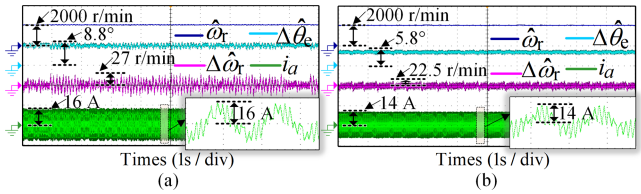

Fig. 8. Steady-state control performance of the sensorless control at 2000 r/min ($N_{ratio} = 6$) under 50% rated load. (a) Conventional SVPWM. (b) Proposed SSDU-SVPWM.

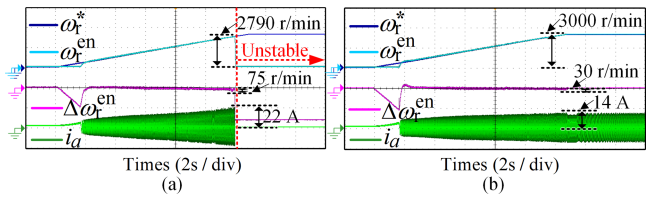

Fig. 9. Extreme test of the sensor control at 3000 r/min speed command ($N_{ratio} = 4$) under 50% rated load. (a) Conventional SVPWM. (b) Proposed SSDU-SVPWM.

the phase current is 16 A. In comparison, the position estimation error of the proposed method is 5.8°, the speed estimation error is 22.5 r/min, and the phase current is 14 A.

The aforementioned experimental steady-state control performance show that, in comparison with the traditional method, the proposed method has merits of smaller phase-current ripple, higher position estimation accuracy, and better steady-state performance.

B. Lowest Carrier Ratio Experiments

Furthermore, to compare the lowest carrier ratio operation, the following experiments from zero speed to a given maximum speed under 50% rated load are implemented. The maximum speed within sensor control is 3000 r/min. Fig. 9(a) shows that the speed of conventional method becomes unstable when it rises to 2790 r/min ($N_{ratio} = 4.3$). Nevertheless, Fig. 9(b) shows that the speed of the proposed method can remain stable even it rises to 3000 r/min ($N_{ratio} = 4$).

Another comparison is performed in sensorless control at the same condition of Fig. 9, as shown in Fig. 10. From Fig. 10(a), when the speed of the conventional method rises to 1650 r/min ($N_{ratio} = 7.3$), the MRAS becomes unstable, and the position error and speed error are 28.4° and 27.5 r/min, respectively. While in Fig. 10(b) with the proposed method, when the speed reaches to 1650 r/min, the position error and

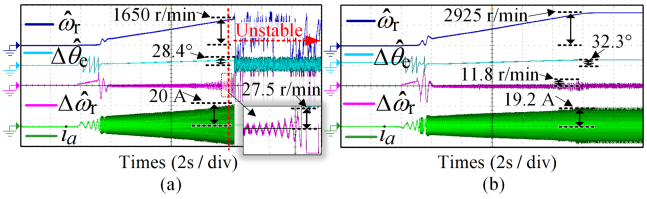

Fig. 10. Extreme maximum speed test of the sensorless control under 50% rated load. (a) Conventional SVPWM. (b) Proposed SVPWM.

speed error of are 24.1° and 4.5 r/min, respectively, which are 4.3° and 23 r/min smaller than those of the conventional method. Then, when the speed rises to 2925 r/min ($N_{\text{ratio}} = 4.1$), the position error and speed error are 32.3° and 11.8 r/min, respectively. The maximum speed of sensorless control with the proposed method is 2925 r/min in comparison with 1650 r/min with the conventional method. In addition, both the conventional method and the proposed method show similar control performance under high carrier ratio and have the same problems of the estimated position/speed oscillation and long convergence time during the standstill start-up in sensorless control.

IV. Conclusion

To solve problems of instability and large current/torque ripple of PMSM drives under low-carrier ratio, a single sampling double update SVPWM strategy is proposed. In this method, considering the rotation angle of the voltage vector during the digital delay and inverter delay, the PWM cycle is divided into the first half and the second half to generate different voltages, thus the accuracy of voltage synthesis is improved. The comprehensive experiments show that the proposed SSDU-SVPWM can improve the stability and efficiency of the PMSM drives under low-carrier ratio. In the case of half-load, the minimum carrier ratio within position sensor control can be reduced to 4, and the minimum carrier ratio within position sensorless control can be reduced to 4.1. In addition, the proposed method is suitable for low-side shunt-resistor current-sensing drives, which is a low-cost current sampling topology and convenient to be implemented. Moreover, the proposed SSDU-SVPWM is a universal modulation method and can be applied to other-type motor drives to enhance the low-carrier ratio operation.

References

[1] C. Li et al., "A modified neutral-point balancing space vector modulation technique for three-level neutral point clamped converters in high-speed drives," *IEEE Trans. Ind. Electron.*, vol. 66, no. 2, pp. 910–921, Feb. 2019.

[2] M. Merdzan, J. J. H. Paulides, A. Borisavljevic, and E. A. Lomonova, "The influence of the inverter switching frequency on rotor losses in high-speed permanent magnet machines: An experimental study," in *Proc. IEEE Int. Electric Mach. Drives Conf.*, 2015, pp. 1628–1633.

[3] S. Zhou, J. Liu, L. Zhou, and Y. Zhang, "DQ current control of voltage source converters with a decoupling method based on preprocessed reference current feed-forward," *IEEE Trans. Power Electron.*, vol. 32, no. 11, pp. 8904–8921, Nov. 2017.

[4] S. Zhu, W. Huang, Y. Yan, and Z. Niu, "High-damped complex vector current regulator for PMSM based on active damping function," *IEEE Trans. Power Electron.*, vol. 38, no. 4, pp. 5204–5216, Apr. 2023.

[5] B.-H. Bae and S.-K. Sul, "A compensation method for time delay of full-digital synchronous frame current regulator of PWM AC drives," *IEEE Trans. Ind. Appl.*, vol. 39, no. 3, pp. 802–810, May/Jun. 2003.

[6] G. Zhang, G. Wang, D. Xu, and Y. Yu, "Discrete-time low-frequency-ratio synchronous-frame full-order observer for position sensorless IPMSM drives," *IEEE J. Emerg. Sel. Topics Power Electron.*, vol. 5, no. 2, pp. 870–879, Jun. 2017.

[7] L. Corradini and P. Mattavelli, "Modeling of multisampled pulse width modulators for digitally controlled DC–DC converters," *IEEE Trans. Power Electron.*, vol. 23, no. 4, pp. 1839–1847, Jul. 2008.

[8] I. Z. Petric, P. Mattavelli, and S. Buso, "Investigation of nonlinearities introduced by multi-sampled pulsewidth modulators," *IEEE Trans. Power Electron.*, vol. 37, no. 3, pp. 2538–2550, Mar. 2022.

[9] H. Ueta and T. Yokoyama, "1MHz multisampling deadbeat control with disturbance compensation method for three phase PWM inverter," in *Proc. Int. Power Electron. Conf.*, 2018, pp. 1883–1889.

[10] Z. Wang et al., "A novel deadbeat predictive current control of permanent magnet synchronous motor based on oversampling scheme," *Int. Eng. Technol. Electric Power Appl.*, vol. 15, no. 8, pp. 1029–1044, Mar. 2021.

[11] P. Yi et al., "PMSM torque ripple minimization based on novel low carrier ratio PWM technique," *IEEE Trans. Power Electron.*, vol. 37, no. 9, pp. 11071–11084, Sep. 2022.

[12] G. Liang et al., "An optimized pulsewidth modulation for dual three-phase PMSM under low carrier ratio," *IEEE Trans. Power Electron.*, vol. 37, no. 3, pp. 3062–3072, Mar. 2022.

[13] C. Wang, K. Wang, and X. You, "Research on synchronized SVPWM strategies under low switching frequency for six-phase VSI-fed asymmetrical dual stator induction machine," *IEEE Trans. Ind. Electron.*, vol. 63, no. 11, pp. 6767–6776, Nov. 2016.

[14] Y. Wang et al., "Deadbeat model-predictive torque control with discrete space-vector modulation for PMSM drives," *IEEE Trans. Ind. Electron.*, vol. 64, no. 5, pp. 3537–3547, May 2017.

[15] J. Riedemann et al., "A space vector modulation strategy for PMSMs operating at low switching-to-fundamental frequency ratio," *IEEE Trans. Ind. Electron.*, vol. 70, no. 11, pp. 11067–11077, Nov. 2023.

[16] V. Blasko, "Analysis of a hybrid PWM based on modified space-vector and triangle-comparison methods," *IEEE Trans. Ind. Appl.*, vol. 33, no. 3, pp. 756–764, May/Jun. 1997.

[17] X. Sun, C. Wu, and J. Wang, "Adaptive compensation flux observer of permanent magnet synchronous motors at low carrier ratio," *IEEE Trans. Energy Convers.*, vol. 36, no. 4, pp. 2747–2760, Dec. 2021.